

David W. Smith · Bruce S. Gardiner
Lihai Zhang · Alan J. Grodzinsky

Articular Cartilage Dynamics

 Springer

Articular Cartilage Dynamics

David W. Smith · Bruce S. Gardiner
Lihai Zhang · Alan J. Grodzinsky

Articular Cartilage Dynamics

 Springer

David W. Smith
Faculty of Engineering and Mathematical
Sciences
University of Western Australia
Perth, WA, Australia

Lihai Zhang
Department of Infrastructure Engineering
University of Melbourne
Melbourne, VIC, Australia

Bruce S. Gardiner
College of Science, Health, Engineering
and Education
Murdoch University
Perth, WA, Australia

Alan J. Grodzinsky
Departments of Biological Engineering,
Electrical Engineering, Computer Science,
and Mechanical Engineering
Massachusetts Institute of Technology
Cambridge, MA, USA

ISBN 978-981-13-1473-5 ISBN 978-981-13-1474-2 (eBook)
<https://doi.org/10.1007/978-981-13-1474-2>

Library of Congress Control Number: 2018953314

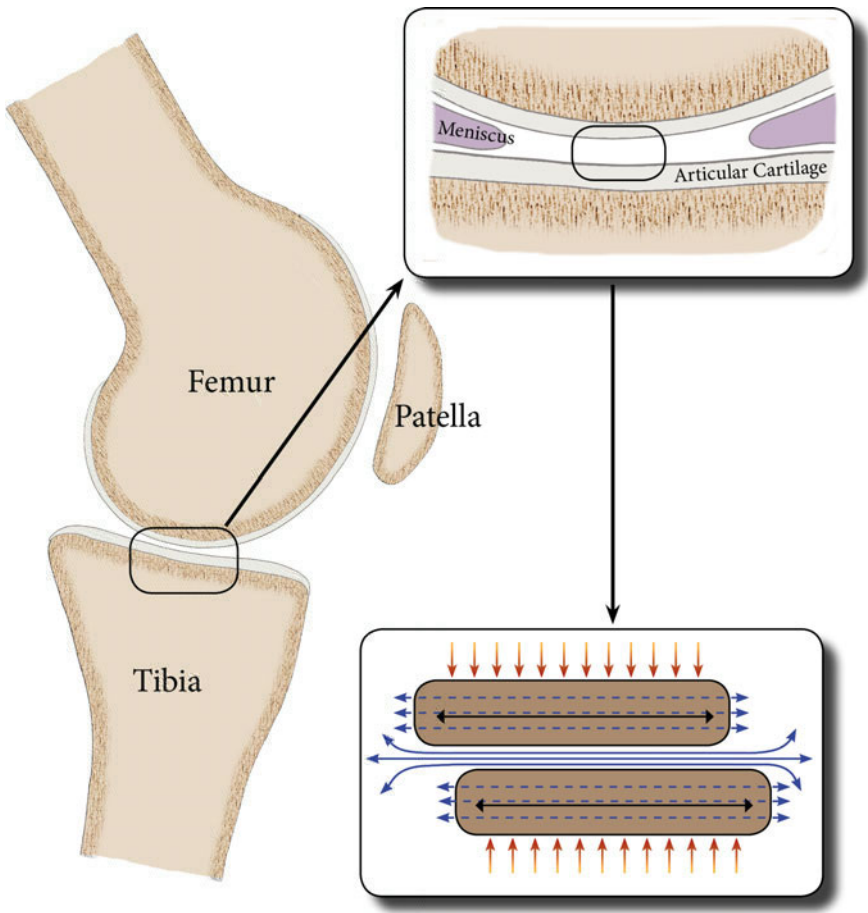
© Springer Nature Singapore Pte Ltd. 2019

This work is subject to copyright. All rights are reserved by the Publisher, whether the whole or part of the material is concerned, specifically the rights of translation, reprinting, reuse of illustrations, recitation, broadcasting, reproduction on microfilms or in any other physical way, and transmission or information storage and retrieval, electronic adaptation, computer software, or by similar or dissimilar methodology now known or hereafter developed.

The use of general descriptive names, registered names, trademarks, service marks, etc. in this publication does not imply, even in the absence of a specific statement, that such names are exempt from the relevant protective laws and regulations and therefore free for general use.

The publisher, the authors and the editors are safe to assume that the advice and information in this book are believed to be true and accurate at the date of publication. Neither the publisher nor the authors or the editors give a warranty, express or implied, with respect to the material contained herein or for any errors or omissions that may have been made. The publisher remains neutral with regard to jurisdictional claims in published maps and institutional affiliations.

This Springer imprint is published by the registered company Springer Nature Singapore Pte Ltd. The registered company address is: 152 Beach Road, #21-01/04 Gateway East, Singapore 189721, Singapore



Foreword

Articular cartilage is found within diarthrodial joints covering the ends of long bones. The two primary mechanical functions of articular cartilage are to reduce the magnitude of contact stresses (the contact area of cartilage on cartilage is much larger than if bone directly contacts bone) and provide a low-friction bearing surface during motion (cartilage on cartilage has a much lower friction coefficient than if bone rubs directly on bone). The reduced contact stress and low friction at the contact interface together minimize internal damage to the cartilage extracellular matrix and resident chondrocytes, as well as minimizing wear damage at the cartilage surface. Fulfillment of these two primary mechanical functions provides the mechanical basis for the cartilage tissue to survive an extremely challenging mechanical environment.

Yet despite the best efforts by joint tissues to maintain themselves, many people develop disease states known collectively as osteoarthritis (OA). OA is a progressive and often disabling disease of the whole joint, involving multiple joint tissues. Over a period of years, the articular cartilage softens and degenerates—the hallmark of OA—leaving bare bone to rub painfully on bare bone. This results in substantial morbidity and much suffering in the general community, as well as generating substantial economic loss due to ill health and/or early retirement. To date, most drug treatments for OA are directed at symptomatic pain relief. It is unfortunate that current drug treatments have no demonstrable impact on altering the rate of structural change within osteoarthritic cartilage.

Even after an enormous research effort around the world over many decades, involving the expenditure of many billions of dollars, no single cause of osteoarthritis has been found. Both fundamental and clinical researchers have concluded that there is in fact no single cause and that OA disease states arise through a variety of pathways. Some osteoarthritic disease pathways to OA involve inflammatory initiators, while other pathways clearly involve mechanical initiators (e.g. joint trauma and overuse syndromes). A common view is that the onset of osteoarthrosis occurs when the recuperative processes within the cartilage and the surrounding tissues are pushed beyond their capacity to maintain tissue homeostasis, due to a patient-specific combination of genetic and environmental factors.

The evidence to date suggests that there are no easy answers and there will be no ‘silver bullet’ that eliminates OA. A more plausible scenario is that avoiding or managing established OA requires advice and treatment on a case-by-case basis—first identifying the specific combination of factors at work in any one individual and then instituting a patient-specific treatment regime. Undoubtedly, the most accurate assessment of disease potential and its management require an evaluation of patient-specific data in the context of a ‘system-level’ understanding of both normal cartilage physiology and OA cartilage physiology, gained from a deep and sustained integration of knowledge grounded in facts gathered over decades of basic biomedical science and clinical research.

It is our view that despite the intensive research efforts over decades, such a system-level understanding of cartilage is largely missing from the current cartilage literature. The focus of much basic research today remains on discovering the components in cartilage (e.g. signaling molecules, genes or protein expression profiles, or discovering the effect of ‘gene silencing’ or disabling protein activity). At a clinical level, there is a focus on high-level statistical correlations between system ‘perturbations’ and system outcomes (e.g. partial meniscectomy and incidence of OA, BMI and the incidence of OA, diabetes and the incidence of OA). Such ‘discovery’ approaches become problematic only because they completely dominate the current research landscape and, like all activities, are subject to the law of diminishing returns (i.e. successive studies yield diminishing increments to our knowledge). Practiced to excess, discovery, epidemiological and clinical research approaches deflect both attention and research funding from the development of integrated understandings of cartilage, which only serve to limit the potential benefits of the hard-won knowledge obtained from the previous discovery and clinical approaches. In short, our contention is there is currently a deficit of knowledge integration in cartilage research. An aim of this book is to help change this situation.

When integrative models of cartilage are employed, too often such models are far too simple. For example, articular cartilage is presented as a static tissue with a very limited capacity to repair—if it has any capacity to repair at all? From this simple conceptual model, it follows logically that cartilage inevitably ‘wears out,’ much like a pair of shoes wear out, and so patients are inevitably in need of joint replacement surgery (usually involving a metal implant of some kind). A large industry has grown up around joint replacement, partly because it is so effective.

But the same conceptual model leads to the conclusion that ‘conservative treatment’ of osteoarthritis is ineffective, and from this, it is a small step to conclude that conservative treatment is simply not beneficial. In practice, most people experience considerable inconvenience, suffering, and loss of income over one or two decades prior to joint replacement, and there is no effective treatment for OA during this long and debilitating period when inactivity, isolation and depression are all too frequent. So-named ‘conservative treatments’ may be able to reduce the high personal costs of this disease, but one barrier to the development of

conservative treatments is conceptual. In their review of osteoarthritis, Vincent and Watt (2018) neatly sum up the core issue:

Many clinicians regard OA as being simply a disease of ‘wear and tear,’ and by implication one in which disease modification is not possible. Such prejudices have led to significant academic apathy in this disease that is reflected not only in our poor understanding of disease pathogenesis, but also in the failure to classify the disease with greater precision and to develop sensitive tools for diagnosis and prognostic assessment.

Another barrier to the development of conservative treatments is the type of business model required to support conservative treatments. It is a truism to observe that much of the modern medicine is geared to acute care, rather than geared to disease prevention or chronic care models—but this should not diminish the importance of either prevention or chronic care. With healthcare systems geared to acute care, conservative treatments almost inevitably play a minor role among the therapeutic options in most advanced healthcare systems around the world today. With many vested interests within the healthcare systems, weak consumer knowledge and little bargaining power in their dealings with acute care specialists, potentially health insurers are the most likely vested interest group capable of leading a rebalancing of healthcare systems toward the prevention and conservative management of chronic diseases. Health insurers already reduced the premiums and so reward those who lead certain lifestyles, but if health insurers realized the potential advantages, quite possibly health insurers might in the future offer funding for ‘integrative research’ of the type presented here.

In this book, we argue for a new, deeper functional understanding of normal cartilage that is offered by the simple ‘use and replace’ model of cartilage described above. The theme throughout the book is that cartilage is not a static tissue, rather, it is a dynamic tissue that adjusts and remodels itself throughout the life to meet the changing environmental demands placed upon it. Unsurprisingly, articular cartilage is much like all tissues in the body [and yes, even brain tissue remodels, and in some parts of the brain, there is even neural cell proliferation (Boldrini et al. 2018; Sahay et al. 2011; Spalding et al. 2013; Pilz et al. 2018)]. However, articular cartilage tissue remodeling occurs over a longer timescale than many other tissues in the body (and often on a timescale much longer than busy modern lifestyles allow us!). For in the absence of a deeper understanding of cartilage tissue physiology, we are severely constrained in the formulation of strategies for maintaining healthy cartilage and for treating diseased cartilage. Without a deeper understanding, palliative care followed by joint replacement is all but inevitable. And in the absence of an integrated framework that explains how the cartilage ‘works’ as a tissue, discovery-based science is left to find new therapies through serendipity. But we know that ignorance of basic tissue and cell physiology is demonstrably an inefficient and very costly way to advance clinical science.

For these reasons, we aim to accelerate the process of developing a logical framework for understanding cartilage tissue by attempting to describe how we believe cartilage successfully operates as a tissue over a lifespan. To develop a more complete and hopefully more useful integrated framework for cartilage physiology

we have to extrapolate beyond the limited experimental data currently available. The conceptual frameworks presented here can be interpreted as an extended hypothesis. We adopt a hypothetico-deductive approach, which enables us to formulate a more subtle and complete understanding of cartilage physiology that has been attempted heretofore. The risk in this approach is overreach. But the potential reward of this approach is that it offers new conceptual frameworks that are essential for the development of integrated models of cartilage behavior. By taking this riskier approach, we hope that new ways to rationally modify tissue responses to preserve cartilage tissue or reduce its rate of degradation will suggest themselves naturally to readers. And using this approach, basic biomedical science can be more rapidly and precisely be applied to clinically important questions.

To both interpolate between sparse data sets and extrapolate beyond existing data sets, we use our backgrounds in systems modeling of cartilage and related tissues, guided by our grounding in various fields of engineering, physics, chemistry, materials science, poroelasticity, and reactive transport. We freely apply engineering, physics, and chemical principles in the context of cartilage, gleaned from our experiments and a wide re-reading of the cartilage literature. Such knowledge helps to constrain the ‘space’ of acceptable solutions. We prefer a ‘Bayesian approach’ to inference (http://en.wikipedia.org/wiki/Bayesian_inference). In other words, our prior beliefs, developed in the engineering sciences, have strongly shaped our interpretation of the literature in order to identify what we believe is the most appropriate a priori models for cartilage (i.e. those interpretations consistent with established principles in the major fields of endeavor noted above). This book can then be interpreted as an attempt to develop rational a priori models (or ‘constructs’ as some prefer to call them) to progress our conceptual understanding of cartilage physiology.

For a ‘Bayesian approach’ to inference, such a priori models are crucial because they provide the basis for the interpretation of new data sets. For a Bayesian approach to science, knowledge is cumulative, with a posteriori models becoming a priori models in the next iteration. This fits nicely with an engineering approach to developing analytic and computational models of systems. This Bayesian approach may be contrasted with a ‘frequentist approach’ to inference, adopted by many scientists, where either a true or false inference is drawn on the basis of ‘statistical tests’ on data: see (http://en.wikipedia.org/wiki/Frequentist_inference). In this frequentist approach to science, a priori knowledge often plays no formal role in inference, as the underlying pattern is to be distinguished from ‘random events’ on the basis of statistical tests that have a pre-determined power and significance levels to control type I and type II errors. But the academic landscape is finally beginning to change, and Bayesian approaches are now becoming well-established, even in Statistics Departments, over the last two decades.

Of course, this does not mean that the extended hypothesis on cartilage physiology developed here is necessarily right—by definition, a Bayesian approach dynamically weights and updates hypotheses (a priori knowledge) given the new evidence and/or new beliefs. Explaining the scientific process, McIntyre (2017) comments on ‘multilevel thinking’:

Similarly, the most powerful, versatile, and innovative scientific thinking uses varieties and hierarchies of models including precise mathematical models and computer codes in partnership with “conceptual” models that are fuzzier, more intuitive, and often not overtly mathematical—perhaps expressed more in words or pictures or even in intuitive feelings. Quite often, the intuitive models are wrong or partly wrong to begin with, until modified as a result of crosschecking against something more precise.

Precisely, the approach we believe is most beneficial and so efficient given our current state of knowledge. Our a priori ‘multilevel’ conceptual models of cartilage integrate many separate hypotheses (some of which are reasonably well established in the existing research literature), while developing others that are more speculative. This approach leads to some obvious conclusions about cartilage (often with the usual response by biologists being ‘of course!’), along with some surprising conclusions and the seemingly inevitable responses from biologists and clinicians: ‘do a (frequentist-designed) animal study or clinical trial to test its significance!’. But doing an animal study or clinical trial is not always possible or advisable. While some frequentist inference is clearly necessary (particularly, in the discovery-led phase of science), to rely on it as much as we do today with decades of research behind us leads to an inefficient and very costly way to progress science from our current state (e.g. many experiments duplicate previous work, or identify false leads that are pursued at considerable cost of limited time and resources) (Ioannidis 2005; Ioannidis 2016). Indeed, for complex systems, application of standard statistical tests can lead to unacceptably high rates of false positives and false negatives (e.g. see the NAS publication: *The Irreproducibility Crisis of Modern Science Report* https://www.nas.org/articles/nas_launches_new_report_the_irreproducibility_crisis). On the other hand, concepts and theories can organize and give meaning to large swathes of experimental data and help flag false interpretations, and by these means increase information gain and improve research efficiency.

Hopefully, government-sponsored funding bodies will come to realize and acknowledge these real costs to the research enterprise of ‘business as usual’ and begin to reduce their reliance on discovery-based biomedical research, rebalancing toward a more appropriate mix of theoretical biology and experimental research that reflects the maturity of biomedical and clinical sciences today. In the future, we expect funding bodies will offer greater support to research that organizes existing knowledge and research that has the goal of embodying the cumulative knowledge of that discipline area, providing a firmer platform for new knowledge creation.

While an essential part of organizing knowledge is about developing reductionist databases (e.g. UniProt), we need to aim higher in our ‘knowledge organization’ endeavor and improve the fidelity of both conceptual and quantitative models of biological systems. While the politics of negotiating change is tortuous, such a change in scientific methodology is all but inevitable as disciplines advance. Indeed, history shows science practiced in its mature phase is led by theory rather than by discovery (e.g. the Higgs boson was discovered theoretically—by Peter Higgs in the 1960s—as a particle in the Standard Model for particle physics. This theoretical prediction was confirmed experimentally in 2013 using the Large Hadron Collider at CERN). Interestingly, signs of a transition in the practice of

biomedical and clinical sciences can be found at the US FDA, which is beginning collaborative agreements to develop new computational tools to ‘virtually test’ new drugs and medical devices (e.g. heart pacemakers) as part of their approval process (<http://www.3ds.com/products-services/simulia/solutions/life-sciences/the-living-heart-project>). Perhaps surprisingly, it is often regulations that most influence the pace of change, rather than rational debate about research funding models.

Despite such cultural differences in the practice of research, we believe the extended hypotheses championed here can provide a useful foundation for thinking about and formulating rational, coherent a priori functional models of cartilage physiology. Adopting this approach can help both wet-laboratory and computational biologists alike and eventually help speed translation into a range of rational therapies employed in the clinical sciences. Where possible, we explain the relevance of our extended hypotheses to clinical science, but in the near term, we expect that the extended hypotheses developed here will be most useful in interpreting new and existing experimental data, in formulating new testable hypotheses, and in helping to direct new experimental and theoretical studies toward the most relevant areas of missing information. We both hope and expect that the approach developed here can be built upon (and of course be modified over time) and that this process will yield additional value from the many billions of research dollars already invested in the cartilage research, as well as yield greater value from the expensive experiments and clinical studies to take place in the future.

This book is organized in the following way:

In Chap. 1, we introduce articular cartilage biology consistent with that found in the literature. It explains what cartilage is, how it works as a biocomposite material, how it deforms, and how cartilage depends on synovial tissue for its nutritional needs.

In Chap. 2, we explain how an aggrecan-collagen network forms in vivo and how they work together to create a functional tissue suited to its in vivo mechanical role. Under repeated cyclic loads, aggrecan, collagen and dozens of extracellular matrix components are continually damaged and so have to be repaired. A key focus is how aggrecan, hyaluronan, the collagen network, and the chondrocyte population together maintain homeostasis of the tissue in vivo. This helps establish a view of articular cartilage as a responsive tissue that can continually adjust to its changing circumstances. While much of this chapter is well supported by the research literature, we touch on some aspects that are more speculative (i.e. meaning there is paucity of direct experimental evidence to support them (e.g.) (i) collagen homeostasis, (ii) radial zonation of the extracellular matrix around chondrocytes, and (iii) ongoing chondrocyte proliferation and migration), but we attempt to make sense of them based on our knowledge of cartilage and in light of our understanding of physical and biological sciences.

In Chap. 3, we propose that articular cartilage is able to adapt to significant changes in its environment. This new view of cartilage is more speculative and really forms an ‘extended hypothesis’ that attempts to answer some of the key unknown questions about cartilage: (i) From where does the superficial zone in adult articular cartilage originate, (ii) what are the failure modes in articular cartilage, and (iii) is aggrecan and collagen really shed to the synovial fluid and what role does this play in maintaining articular cartilage health?

In Chap. 4, we explain the technical basics of our current understanding of cartilage lubrication. Clearly, lubrication of the joint is very important functionally, for without adequate lubrication, cartilage surfaces roughen, wear rates increase, and the cartilage tissue may progress toward osteoarthritis. We distill a complex set of ideas and principles into something that is coherent using the principle of effective stress and show that that weeping lubrication and a type of boosted lubrication together ensure articular cartilage minimizes wear.

Chapter 5 explains a number of ‘systems approaches’ for understanding biological tissues. This chapter contains a reasonably detailed account of the cell–cell signaling systems operating in cartilage and a briefer account of the intracellular signaling systems operating inside chondrocytes. It also contains higher-level conceptualisations drawn from other disciplines to aid our understanding of cartilage tissue at a system level.

Chapter 6 explains in detail the meaning of osmotic pressure, Donnan osmotic pressure, and effective stress. We explain the relationships between physical chemistry and articular cartilage mechanics. The chapter begins the process of building a rational, quantitative framework from first principles, which complements biological methods of cartilage investigation.

Chapter 7 presents a large deformation, continuum framework for quantitative modeling of cartilage, using poroelastic modeling as a starting point. This model can be extended as far as a research question might require (e.g. to poro-visco-elasto-plastic models with or without fiber reinforcement with reactive transport).

We hope you enjoy joining us on this demanding but exciting journey, and moreover, we hope that this book forms the basis of ongoing thought-provoking discussions about how cartilage functions as a dynamic tissue.

WA, Australia
WA, Australia
VIC, Australia
MA, USA

David W. Smith
Bruce S. Gardiner
Lihai Zhang
Alan J. Grodzinsky

References

- Boldrini, M., Fulmore, C. A., Tartt, A. N., Simeon, L. R., Pavlova, I., Poposka, V., et al. (2018). Human hippocampal neurogenesis persists throughout aging. *Cell Stem Cell*, 22, 589–599.
- Ioannidis, J. P. (2016). Why most clinical research is not useful. *PLoS Medicine*, 13, e1002049.
- Ioannidis, J. P. A. (2005). Why most published research findings are false. *Plos Medicine*, 2, 696–701.
- Pilz, G. A., Bottes, S., Betizeau, M., Jorg, D. J., Carta, S., Simons, B. D., et al. (2018). Live imaging of neurogenesis in the adult mouse hippocampus. *Science*, 359, 658–662.
- Sahay, A., Scobie, K. N., Hill, A. S., O’carroll, C. M., Kheirbek, M. A., Burghardt, N. S., et al. (2011). Increasing adult hippocampal neurogenesis is sufficient to improve pattern separation. *Nature*, 472, 466–U539.
- Spalding, K. L., Bergmann, O., Alkass, K., Bernard, S., Salehpour, M., Huttner, H. B., et al. (2013). Dynamics of hippocampal neurogenesis in adult humans. *Cell*, 153, 1219–1227.
- Vincent, T. L. & Watt, F. E. (2018). Osteoarthritis. *Medicine*, 46, 7

Acknowledgements

The authors are especially grateful to Ms. Yvette Harrap, who has worked tirelessly to help bring this book to completion in numerous ways, including providing artwork for the front-piece, particularly in Chaps. 4 and 6. We are also grateful to Dr. Saeed Miramini who has done numerous numerical simulations and to Associate Professor Piaras Kelly, who kindly checked the equations for introductory remarks on large deformation poromechanics. The authors take responsibility for any remaining errors.

Contents

1	Introduction to Articular Cartilage	1
1.1	Setting the Scene	1
1.2	Where Is Articular Cartilage Found?	8
1.3	How Is Hyaline Cartilage Described Histologically?	9
1.4	What Is the Composition of Hyaline Cartilage?	16
1.5	Cartilage Is a Biocomposite Material	25
1.6	How Does Cartilage Deform When Compressed?	33
1.7	The Synovial Fluid and Synovial Membrane	49
1.7.1	What Are the Implications for Osteoarthritis?	54
2	Cartilage Tissue Homeostasis	65
2.1	Introduction	65
2.2	Overview of Cartilage Homeostasis	67
2.3	Aggrecan: Homeostasis and Turnover of Extracellular Matrix	75
2.3.1	Oxygen and Aggrecan Production	75
2.3.2	Aggrecan Homeostasis	77
2.3.3	Aggrecan Turnover	92
2.4	Hyaluronic Acid: Homeostasis and Turnover of Extracellular Matrix	101
2.4.1	Introduction	101
2.4.2	Hyaluronic Acid Homeostasis	102
2.5	Collagen: Homeostasis and Turnover of Extracellular Matrix	104
2.5.1	Introduction	104
2.5.2	The Evolution of the Collagen Network	104
2.5.3	Collagen Protection	112
2.5.4	Collagen Turnover	124
2.6	Overview Collagen Network Repair Mechanisms	133
2.7	Chondrocyte Proliferation and Apoptosis	136
2.8	Chondrocyte Proliferation and Migration	151

- 2.9 Modes and Mechanisms of Chondrocyte Migration 155
 - 2.9.1 Fast Mode Chondrocyte Migration 155
 - 2.9.2 Slow Mode Chondrocyte Migration 159
 - 2.9.3 The Relationship Between Fast and Slow Migration Modes 168
 - 2.9.4 A Mechanism that Explains Slow Mode Chondrocyte Migration 169
 - 2.9.5 Imbalances Between Chondrocyte Proliferation and Chondrocyte Migration 187
- 2.10 Radial Zonation Around Chondrocytes 190
 - 2.10.1 How Can ECM Synthesis and Degradation Occur Simultaneously? 190
 - 2.10.2 Uncovering the Chemical Principles for Self-organization of the ECM 193
 - 2.10.3 Chemical Principles for Self-organization of the ECM 203
 - 2.10.4 MMPs, Aggrecanases, TIMPs, Cathepsins, and Cystatins 209
 - 2.10.5 Aggregate 221
 - 2.10.6 Collagens 223
- 2.11 What Are the Implications for Osteoarthritis? 234
- 3 Cartilage Tissue Dynamics 245**
 - 3.1 Introduction 245
 - 3.2 Overview of Cartilage as a Dynamic Tissue 247
 - 3.3 Material Failure Modes Within the Cartilage Biocomposite 247
 - 3.4 Aggrecan Shedding to the Synovial Fluid 259
 - 3.5 Collagen Network Shedding to the Synovial Fluid 265
 - 3.6 The Cartilage Surface 282
 - 3.7 Dynamics of the Calcified Cartilage Zone 286
 - 3.8 Dynamics of Subchondral Bone 292
 - 3.9 Transport of Signaling Molecules Across the Osteochondral Junction 303
 - 3.10 What Are the Implications for Osteoarthritis? 305
- 4 Lubrication, Friction, and Wear in Diarthrodial Joints 311**
 - 4.1 Introduction 311
 - 4.2 Friction 314
 - 4.3 Soft Porous Bearings 317
 - 4.3.1 Hydrodynamic Lubrication 317
 - 4.3.2 Consolidation of Two Loaded Cartilage Plates 319
 - 4.3.3 Boundary Lubrication 322

- 4.3.4 Mixed-Mode Lubrication 327
- 4.4 Experimental Data Relating to Cartilage Friction 340
- 4.5 Cartilage Inspired Artificial Porous Bearing 355
- 4.6 Fundamental Hypotheses for Clinical Biomechanics and the Relevance to Osteoarthritis 355
- 5 A Systems Approach to Articular Cartilage 361**
 - 5.1 Introduction 361
 - 5.2 Networks and Basic Functional Units in Tissues 362
 - 5.3 Growing to Understand Networks in Organisms 366
 - 5.4 Objective Functions, Set-Points and Regulating Chondrocyte Behavior in Articular Cartilage 371
 - 5.5 Negative Feedback and Set-Points 375
 - 5.6 Extracellular Signaling Systems in Cartilage 379
 - 5.6.1 TGF β Signaling 379
 - 5.6.2 Ihh-PTHrP Signaling 383
 - 5.6.3 Wnt Signaling 390
 - 5.6.4 IGF Signaling 395
 - 5.6.5 OPG-RANKL-RANK Signaling 397
 - 5.6.6 IL-1, TNF α , Nitric Oxide and Prostaglandins 398
 - 5.6.7 HIF Signaling 399
 - 5.6.8 IL-6 Signaling 400
 - 5.6.9 BMP Signaling 400
 - 5.6.10 FGF Signaling 400
 - 5.6.11 Integrin Signaling 401
 - 5.6.12 Purinergic Signaling 402
 - 5.6.13 Calcium Signaling 403
 - 5.6.14 Toll Signaling 404
 - 5.6.15 RAGE Signaling 406
 - 5.6.16 Heparin Sulfate Proteoglycans 407
 - 5.6.17 Periostin Signaling 408
 - 5.7 Intracellular Signaling Pathways 408
 - 5.8 Interactions Between Endocrine, Paracrine and Autocrine Factors, Signaling Pathways, Transcription Factors and MicroRNAs 411
 - 5.8.1 General Observations on Interactions Between Systemic and Local Signaling 411
 - 5.8.2 Interactions and Growth Factors 418
 - 5.8.3 Interactions Between Signaling Pathways 419
 - 5.8.4 Transcription Factors in Cartilage 420

5.9	How Can a Systems Approach Progress Cartilage Research?	421
5.10	What Are the Implications for Osteoarthritis?	424
6	Osmotic Pressure, Solid Stress, and the Diffuse Double Layer	429
6.1	Introduction	429
6.2	Osmotic Pressure	430
6.3	Donnan Osmotic Pressure	439
6.4	Solid Stress or Effective Stress	444
6.5	Osmotic Pressure for Non-ideal Solutions	454
6.6	Cell Models for Polyelectrolyte Solutions	457
6.7	Pressure Measurement for Solutions and Tissues	461
7	Theory for Modeling Articular Cartilage	469
7.1	Introductory Remarks on Solid Mechanics and Poromechanics	469
7.2	Poroelasticity	490
7.2.1	Terzaghi's 'Principle of Effective Stress' and 1-D Consolidation Theory	490
7.2.2	Biot Poroelasticity Theory	517
7.2.3	Drained and Undrained Poroelastic Responses	521
7.2.4	Equilibrium Equations for Large Deformation of a Porous Medium	522
7.2.5	Nonequilibrium Equations for Large Deformation of a Porous Medium	527
7.2.6	Transport Equations for Large Deformations of Porous Media	531
7.2.7	Boundary and Initial Conditions	541
7.3	Poroelastic Modeling of Cartilage	542
7.3.1	Introduction	542
7.3.2	The Definition of Effective Stress and Water Flow in Cartilage	543
7.3.3	Aggrecan Transport Through Cartilage	547
7.3.4	The Compressibility of Aggrecan in Cartilage	552
7.3.5	Representing the Tensile Strength of Collagen in Cartilage	556
7.3.6	The Storage Equation for Cartilage	558
	Appendix A: Key Concepts for Biology	561
	Appendix B: Why Are Biological Systems so Complex?	585
	Appendix C: The Formation of Diarthrodial Joints and Articular Cartilage	589

Appendix D: The Compressive Stiffness of Glycosaminoglycans 595

**Appendix E: Estimating the Aggrecan Production Rate, Aggrecan
Turnover and Aggrecan Flux Through the Surface of
Knee Articular Cartilage** 605

**Appendix F: GAG and Aggrecan Flux Through Surface of Knee
Cartilage** 609

Appendix G: The Rate of Volume Change in Material Coordinates. 611

Appendix H: The Cauchy Stress Tensor 613

Appendix I: Terzaghi’s Principle of Effective Stress 615

**Appendix J: The Momentum Balance Equation and Strain
Work Rate** 619

Appendix K: State Variables, Entropy, and Free Energy Potentials 625

Appendix L: A Free Energy Potential for Aggrecan 655

Appendix M: Diffusive Transport of Aggrecan 661

**Appendix N: Stress and Elasticity Tensors in a Fiber-Reinforced
Composite** 665

Appendix O: The Storage Equation for Cartilage 669

References 673

List of Figures

Fig. 1.1 Low magnification epifluoroscope images of bovine (1–2 years old) articular cartilage labeled for actin microfilaments (Langelier et al. 2000). Image **a** is for cartilage subject to load-bearing contact forces on its top surface (top of image), while Image **b** is for a more peripheral region of cartilage that experiences reduced load-bearing contact forces. Both images are segmented by horizontal lines into superficial, middle, and deep zones. Note that Image **a** has a higher cell density than Image **b**, indicating more highly loaded regions of tissue experiencing larger strains require (*and have*) greater proliferative capability and ECM repair capacity, so as to maintain the integrity of the tissue. Consistent with this interpretation, Image **a** shows greater ongoing proliferation than Image **b**, as a greater proportion of chondrocytes is arranged in ‘proliferative columns’ in both the deep and middle zones. In addition to differences in cell density and proliferative drive, centrally located (porcine) chondrocytes contain about twice as much aggrecan mRNA as lateral chondrocytes, and upon loading central chondrocytes increases aggrecan mRNA about twice as much as similarly loaded lateral chondrocytes (Bevill et al. 2009) 10

Fig. 1.2 Scanning electron micrograph of a freeze fracture showing normal human articular cartilage on osteoporotic subchondral bone in 76 year old (Li et al. 1999). Scale bar equals 100 μm. Image **a** shows sheet-like structures revealed by the freeze fracture preparation imaged in backscatter mode, while Image **b** shows the same surface in scanning electron mode (showing more clearly the irregularities in the 3D surface). Further high-resolution (7T) MRI of human knee tibial cartilage can be found in Goodwin et al. (2004). 12

Fig. 1.3 Scanning electron microscope image of collagen network in [femoral] cartilage showing fibrillar entwinement in the extracellular matrix. Scale bar 2 μm (Nickien et al. 2013; Broom et al. 2001). See also Figs. 2, 4, 6, 7, and 8 in Nickien et al. (2013) and Figs. 3, 7, 8, and 9 (Broom et al. 2001) 20

Fig. 1.4 Drawing of image shown in Fig. 3 of Vaughan et al. (1988) showing rotary shadowed cartilage fibril. The fibril in this shadow appears to be sheathed in collagen type IX. The globular amino-terminal domain (1) and a short non-collagenous domain (NC3), which gives rise to a prominent kink (2) in the otherwise relatively rigid collagenous portion, are notable features also visible in the molecules on the fibril surface (Vaughan et al. 1988). Note collagen fibril shown in Vaughan et al. (1988) is about 35 nm in diameter. Figure sketch drawn by Yvette Harrap. See also Fig. 3 (Broom et al. 2001), which shows an SEM image with the (tiny) globular amino-terminal domains collapsed into the collagen fibrils, and Fig. 1.5 21

Fig. 1.5 Schematic of the 10 + 4 microfibril structure of a thin cartilage collagen fibril. A pair of collagen XI microfibrils comprise half of a four microfibril cores surrounded by ten microfibrils at the surface. The collagen XI/IX/II assembly is a cross-linked heteropolymer, as is V/I, and is an important component of the fibril assembly mechanism. Blue: collagen II molecules; yellow: collagen XI molecules; red: collagen IX molecules. The N-terminal thrombospondin-like domains of collagen XI (yellow) are shown extending from the core microfibrils onto the fibril surface (Kadler et al. 2008) (model kindly provided by Dr David Eyre, University of Washington, Seattle). Such a prototypical fibril is about 20 nm in diameter (Gottardi et al. 2016). Thicker fibrils are formed by winding two or more prototypical fibrils together (so a 100-nm fibril is formed from about 7 prototypical 20 nm fibrils) 22

Fig. 1.6 Atomic force microscope image of the fetal aggrecan molecule (generated by AFM in ‘tapping mode’), showing protein core with GAG molecules attached (via linker protein) clearly visible (N and C denote N-terminal and C-terminal regions of the core protein) (Ng et al. 2003). Scale bar approximately 50 nm 23

Fig. 1.7 Combined properties of collagens and aggrecan in cartilage (Kiani et al. 2002). See also Fig. 4 (Roughley and Mort 2014) 28

Fig. 1.8 Stress–strain behavior of the cartilage composite is the sum of the collagen network stress–strain curve (depicted here as

bilinear for simplicity, but more generally is nonlinear) and a nonlinear stress–strain curve for aggrecan. Initially, there is a tensile prestress in the collagen network and a compressive prestress in the aggrecan network. With no load on the cartilage surface, these two stresses are self-equilibrating ($\sigma_{\text{initial}}^c = \sigma_{\text{initial}}^t$ at $\varepsilon = 0$). Interestingly, we see that upon loading of the cartilage surface, the initial stiffness of the cartilage composite is greater than either the stiffness of the collagen alone or the stiffness of the aggrecan alone (i.e. $E_{\text{composite}} > E_{\text{collagen}} > E_{\text{aggrecan}}$). At large tensile strains, the stiffness of the cartilage composite approaches the stiffness of the collagen network. For compressive strains greater than the initial collagen network strain ($\varepsilon_{\text{initial}}^{\text{col}}$), the cartilage composite assumes the compressive stiffness of the aggrecan. We note that a similar ‘compression curve’ is reported experimentally [see, for example, Fig. 8a

(Chahine et al. 2004)] 29

Fig. 1.9 In situ, volume changes and fluid flux during [static, normal] loading [of the patellofemoral joint at 60° flexion] with 150% body weight [measured maximum contact pressure 3.6 MPa]. The error bars show one standard deviation of the variability between individuals [there are six samples tested]. **a** Volume change of the patellar cartilage (3D analysis), **b** rate of fluid loss from the interstitial patellar cartilage matrix per square centimeter surface area (and fluid microns/s), based on the assumption that during compression the fluid flow will occur through the articular surface into the joint cavity. A 43% fluid loss was observed from the interstitial matrix after 3.5 h of static loading, the fluid flow rate per square centimeter articular surface being initially $1.3 (\pm 0.5) \text{ mm}^3/\text{min cm}^2$ ($0.217 \pm 0.083 \text{ }\mu\text{m/s}$) for the first 14 min after loading, and $0.22 (\pm 0.04) \text{ mm}^3/\text{min cm}^2$ ($0.037 \pm 0.007 \text{ }\mu\text{m/s}$) in the terminal phase of the experiment (>120 min) (Herberhold et al. 1999). *Note* The timescale on diagram (**b**) appears to be minutes rather than seconds, as indicated by the figure caption. In other words, even after 3.5 h of steady loading, the cartilage was still consolidating, albeit at a slow rate 35

Fig. 1.10 Representative sample of (dog) cartilage with initial height 0.6 mm (shaved 0.1 mm thick) under various compression levels [zero strain, 12.5, 24, and 29% engineering strain (where the ‘engineering strain’ is defined as the change in specimen height divided by the initial specimen height)]. The circles correspond

to cells that were tracked through the increasing compression in the superficial zone (0–60 μm) (A), transitional zone (61–180 μm) (B, C), and deep zone (181–600 μm) (D, E) 10× magnification (Szarko and Xia 2012). 36

Fig. 1.11 Graph summarizing the depth-dependent properties of intratissue strain within the three bulk tissue strain levels (12.5, 24, and 29% [i.e. superficial zone, transitional zone, and deep zone (DZ)]). Significantly decreased intratissue strains were seen with increasing tissue depth. Intratissue strains also significantly increased with increasing bulk tissue strains (although the increase in the DZ was only significant upon 29% bulk tissue strain). The * symbol indicates significance at the $p < 0.05$ level (Szarko and Xia 2012). Based on reported stress–strain responses (Szarko and Xia 2012), it is interesting to note that the equilibrium cartilage stiffness in dog humeral head cartilage at 29% average Young’s modulus (deep zone) is measured to be around 0.165 MPa (stress)/0.04 (strain) = 4.1 MPa. 37

Fig. 1.12 A typical combined testing curve. [Osteochondral plugs consisting of] cartilage and bone were tested to a load resulting in 0.5% bone strain. The stiffnesses of cartilage and bone were determined as the tangent to the loading curves at 0.45% bone strain Rohl et al. (Ding et al. 1998a). Note that the osteochondral plugs tested are specimens 7.5 mm in diameter with a bone length 8.5 mm (which included 7.5-mm trabecular bone beneath the subchondral bone plate). The samples are tested unconfined, with a preload of 0.09 MPa. 20 cycles of preconditioning applied at 5 mm/s (i.e. around 0.02 and 0.03 cartilage strain per second, a complete load cycle took between 3 and 6 s, so preconditioning took between 1 and 2 min), prior to the test loading (a typical test loading stress–strain curve is shown above). Mean thickness of normal cartilage was 2.5 mm (range 1.7–3.6 mm). Mean thickness of early stage osteoarthritis cartilage is slightly thinner at 2.3 mm (range 1.8–3.0 mm). 39

Fig. 1.13 Stress–strain response for a typical specimen [bovine cartilage (3 months to 3 years of age) explants plugs, 3 mm in diameter and 1.8 mm in height, which were tested under unconfined compression with impermeable platens and free draining sides], at various loading frequencies. Loads ranged from zero to a nominal 5.7 MPa, while the engineering strain in the load direction ($1 - \lambda_3$) ranged about 12% seating strain to total loading strain of 34% (a difference of about 22%, as shown above) (Park et al. 2004). 44

Fig. 1.14 Phase φ of the dynamic modulus [i.e. the inverse tangent of the ratio of the energy loss to energy stored in the cartilage] for both normal and GAG-depleted cartilage obtained by AFM-based dynamic indentation is compared with the phase angle from macroscopic unconfined compression tests using 3-mm diameter by 1-mm-thick cartilage disks. The length scales involved in the AFM-based dynamic indentation are: probe radius $R = 12.5 \mu\text{m}$, $\delta_0 = 2 \mu\text{m}$, and probe tip-cartilage contact distance $d = 14 \mu\text{m}$. The relevant length scale for the unconfined compression is the diameter of the sample, $d = 3 \text{ mm}$. As we observed a shift in φ in AFM-based indentation after GAG depletion, a similar shift in the phase φ is expected at physiological macroscales. However, due to experimental limitations in measurements at low frequency, this macroscale hypothesis has yet to be reported for sinusoidal testing (Nia et al. 2013). We note in passing that the shift in φ higher with aggrecan loss is due to an increase in the coefficient of consolidation (i.e. an increase in the product of permeability and equilibrium stiffness) with aggrecan loss. The increase in the coefficient of consolidation is due to the rate of increase in permeability eventually ‘outpacing’ the rate of decrease in aggrecan stiffness as aggrecan concentrations are lowered 45

Fig. 1.15 Cartilage contact characteristics during the stance phase of gait: **a** peak cartilage contact [‘deformation,’ i.e. average strain across both cartilages in mm/mm) and **b** cartilage contact area on the medial and lateral tibiofemoral compartments. Error bars indicate standard deviations. Asterisk denotes significant difference at $p = 0.05$. Because of the numerous comparisons, we only present the relevant comparisons, i.e. between the maximal and minimal values (Liu et al. 2010) 47

Fig. 1.16 Peak tibiofemoral contact deformation for all flexion angles in the medial (blue bars) and lateral (yellow bars) compartment (* denotes statistical significance for $P < 0.05$) (Bingham et al. 2008) 48

Fig. 1.17 MRI of anterior knee synovial recesses, showing synovial fluid (white). **a** Sagittal T2*W GE image showing synovial fluid in the suprapatellar pouch (arrows) and suprahoffatic recess (arrowhead). **b** Sagittal T2*W GE image showing synovial fluid in the infrahoffatic recess (arrow) 50

Fig. 1.18 Tip of synovial villus from a horse (scale bar 20 μm). Note region containing central vessel and PGP 9.5 stained ‘dendritic cells’ extending processes to the villus surface (Kitamura et al. 1999) 50

Fig. 1.19 LHS near-normal femoral articular cartilage (female 60 years, Collins Grade 1 (Muehleman et al. 1997); Grade 0 is normal while Grade 4 is end-stage OA. RHS osteoarthritic femoral articular cartilage (female 54 years, Collins Grade 3). We thank the Gift of Hope Organ and Tissue Donor Network (Itasca, IL) and donor families for human articular cartilage and Dr. Arkady Margulis for tissue procurement. 54

Fig. 2.1 Summary of in situ changes due to load-induced injury. The loss of 7D4 and safranin-O is located in the superficial and middle zones. Increased levels of MMP-3 are co-localized with cell death and broken collagen. The increased 3B3(-) and 7D4 staining in the deep zone indicates an alteration of GAG (Lin et al. 2004) 70

Fig. 2.2 GAG release in response to single impact mechanical loading of cartilage explants. Cartilage explants were loaded in unconfined compression to 14 MPa (resulting in about 30% impact strain) and cultured for 96 h. Cumulative sulfated GAG release was measured by 1,9-dimethylene blue assay. The results are expressed as a % of total explant GAG content per mg and represent mean values from eight explants in each group from three separate experiments (separate donors) (D’Lima et al. 2001) 77

Fig. 2.3 Cartilage explants obtained from 1- to 2-year-old steers, subject to 40 cyclic loads over 20 min. Denatured type II collagen and **GAG** release to media during culture after loading: collagen II fragments (**a**) and **GAG** (**b**) released to culture medium after cyclic loading were assessed. Loading occurred on day 0 on these graphs and the day 0 point represents fragments found in the medium from the 48-h (**a**) or 24-h (**b**) period before loading. There is an increased release of denatured collagen type **II** and of **GAG** to the culture medium after loading compared to unloaded controls. **p* < 0.005 comparing loaded to control (Thibault et al. 2002) 78

Fig. 2.4 Fluorescence microscopy of osteochondral tissue sections (-0.5 mm thickness) after incubation in fluorescein diacetate. Fluorescence signal indicates the locations of metabolically active cells 3 days after mechanical compression had been applied to osteochondral explants. Compression was characterized by: **a** 3.5 MPa peak stress at 3×10^{-5} strain rate per second; **b** 7.0 MPa peak stress at 3×10^{-5} strain rate per second; **c** 14 MPa peak stress at 3×10^{-5} strain rate; **d** 14 MPa peak stress at 0.7 strain rate per second. Bar = 200 μ m (Quinn et al. 2001). This data illustrates that higher compressive stresses lead to more cell death, and for physiologically

relevant loading rates, slow rates of loading are much more damaging than faster loading rates (compare **a–c** with **d**). This outcome can be explained by cartilage stiffening as the rate of loading increases, so reducing the amount of strain for a constant loading and so the amount of damage (see discussion on stiffening Sect. 1.6) 80

Fig. 2.5 Radiolabel incorporation during 12 h static compression. ³H-proline (square) and ³⁵S-sulfate incorporation (dot) are expressed relative to incorporation into disks held at 1 mm (the original explant thickness); free-swelling controls were incubated in 24-well culture dishes. All points are mean ± SEM (*n* = 9–12) (Sah et al. 1989). Note the substantial decrease in aggrecan and collagen synthesis with sustained compression 81

Fig. 2.6 Effect of dynamic compression on the dose response of IGF-I (for one- to two-week-old bovine cartilage obtained from femoropatellar groove). Shown here is incorporation of [³H]-proline (**a**) and [³⁵S]-sulfate (**b**) into cartilage disks treated with 0, 3, 10, 30, 100, or 300 ng/ml IGF-I in the absence (square) or presence (dot) of a 2% sinusoidal strain imposed at 0.1 Hz for 48 h. Data is represented as mean ± S.D. for *n* = 4 samples (Bonassar et al. 2001). Notice that sustained cyclic loading (even at just 0.1 Hz), significantly stimulates aggrecan and collagen production. 82

Fig. 2.7 Effects of dynamic compression on proteoglycan synthesis and deposition on a cell-length scale. Grain density is expressed as a function of distance from the cell membrane *d* averaged over all [radial directions (mean ± SEM, *n* = number of cells sampled)]. Frequencies of applied compression included 0 Hz (**a–c**), 0.01 Hz (**d–f**), and 0.1 Hz (**g–i**). Cells were sampled as a function of radial position *R* within explants, and include those derived from central (**a, d, g**), intermediate (**b, e, h**), and radial edge (**c, f, i**) regions. Values different from those for 0 Hz (by two-tailed Student’s *t*-test; all observed differences were increases) are indicated by *q* (*P* < 0.05) or *w* (*P* < 0.01) (Quinn et al. 1998). 8 h ³⁵S pulse was applied at end of 24 h of cyclic loading. Notice that aggrecan production is significantly enhanced toward the outside of the cartilage disk, where fluid flow is greatest, particularly when the frequency increased to 0.1 Hz. 83

Fig. 2.8 Schematic representation of the in vivo mechanical environment of articular cartilage under intermittent joint loading and motion (Carter et al. 2004) 84

- Fig. 2.9 Bovine animals 10–14 months old, cartilage from humeral head. **a** The RHT-derived chemographic grain density was obtained as a function of distance from the articular surface by analyzing digitized images similar to the photos in Fig. 2.1 using a method developed previously for quantitative autoradiography. **b** Analysis of papain-digested tissue sections from different tissue depth regions using the cationic DMB spectrophotometric agent is represented as equivalent chondroitin sulfate concentration determined by a chondroitin sulfate standard. Solid lines with data points and standard errors show the results of one experiment containing 10 specimens; broken line shows the results of an independent prior experiment also containing 10 specimens. Both grain density and equivalent chondroitin sulfate concentration increase with depth. **c** The ratio of grain density to equivalent chondroitin sulfate concentration as a function of depth found using the data from **a** and **b** of this figure. The ratio is not constant and is a function of distance from the articular surface, possibly because the binding chemistry in dense tissue sections of cationic species such as RHT and DMB may be different from that in dilute solution (Buschmann et al. 2000). We note that a similar depth-dependent aggrecan production profile is found in adult human articular cartilage (Maroudas 1975) 87
- Fig. 2.10 **a, b** Cumulative sGAG loss from bovine cartilage to the medium in response to 8-day treatments without or with initial mechanical injury. **c, d** Bovine chondrocyte biosynthesis measured during day 6–8 as ³⁵S-sulfate incorporation rate for the same cartilage disks as in **a** and **b**, respectively. Values are mean ± 95% confidence interval; **a, c** *n* = 3 animals (6 disks/animal); **b, d** *n* = 4 animals (4–6 disks/animal); **P* < 0.001 (Li et al. 2013). 89
- Fig. 2.11 The effects of dynamic compression on bovine chondrocyte gene expression after 48 h of treatment with exogenous cytokines (normalized cell expression on vertical axis, and no dynamic loading, strain of 10, 20, and 30% on the horizontal axis). For each condition, six cartilage disks from the same animal were pooled for mRNA extraction; *n* = 4 animals. Gene expression levels were normalized to that of the 18S gene and then normalized to the no-cytokine, no compression control condition which had an expression level = 1. Data is presented as mean ± 95% confidence interval, **P* < 0.001 compared with untreated control; #*P* < 0.001 compared with cytokines-alone treatment (Li et al. 2013) 90

- Fig. 2.12 Model depicting the potential protective effects of physiological mechanical stimuli in chondrocytes stimulated with interleukin-1 β (IL-1 β). Moderate mechanical loading induces a number of signaling cascades which leads to the production of extracellular matrix components. Mechanical loading will stimulate integrin-mediated release of interleukin-4 (IL-4) via actin cytoskeleton, mechanical perturbation of stretch-sensitive calcium or sodium channels, or stimulation of a purinergic pathway involving ATP release and subsequent purinoreceptor (P2) or cAMP activation. The loading-induced calcium may cause instability of inducible nitric oxide synthase (iNOS) mRNA or increase transport of interleukin-4 (IL-4), which blocks catabolic effects. In the presence of IL-1 β , mechanical stimuli inhibit cytoplasmic dissociation of NF κ B from inhibitory κ B- α (I κ B- α), which prevents nuclear translocation of the p65/p50 dimers and/or proteolytic degradation of I κ B- α by I κ B-specific kinases (IKK) or impair I κ B- α degradation, thereby switching off transcription for the pro-inflammatory genes (Bader et al. 2011) 91
- Fig. 2.13 Aggrecan cleaved by aggrecanases and matrix metalloproteinases (MMPs). Aggrecan core protein has three globular domains (G1, G2, and G3). The N-terminal G1 domain interacts with hyaluronan with the help of a link protein. G1-VDIPEN³⁴¹ and G1-NITEGE³⁷³ are G1-bearing N-terminal products generated by MMPs and aggrecanases, respectively. Sites cleaved by aggrecanases are shown as (A)–(E), and sites cleaved by MMPs are shown as 1–6. The dotted arrows are sites predicted based on SDS-PAGE analysis of Little et al. (2002) and of Sandy and Verscharen (2001). *KS* keratan sulfate-rich region; *CS* chondroitin sulfate-rich region. Residues and numbering in parentheses indicate bovine sequences. From Nagase and Kashiwagi (2003) 97
- Fig. 2.14 Concentrations of **a** ARGs fragments, **b** sulfated glycosaminoglycan (sGAG), and **c** aggrecan in the study groups healthy knee reference, acute inflammatory arthritis (AA), acute knee injury (AI), chronic knee injury (CI), and knee osteoarthritis (OA). The boxes define the 25th and 75th percentiles with a line at the median, error bars defining the 10th and 90th percentiles and circles represents individual outliers. Note that in panel (**a**) the median level of the chronic injury group is the same as the lower limit of the box; 0.5 pmol ARGs/ml. After Bonferroni correction, *P* values below 0.013

are considered significant to retain the 0.05 overall significance level (Larsson et al. 2009). 99

Fig. 2.15 Redrawn from Benninghoff who described this figure as: ‘a schematic representation of the principal direction of the collagen fibrils in joint cartilage. The chondrons are represented as black ellipses’ (Nickien et al. 2013) 105

Fig. 2.16 Presentation of the collagen network organization in maturing articular cartilage based on articular cartilage from rabbit, pig, and sheep. When maturing, a non-organized collagen fibril network slowly forms into the traditional described zonations (superficial, transitional, and deep), and a Benninghoff-type arcade structure may develop in some animals (including humans). At the same time, cartilage thickness is decreased (Julkunen et al. 2013). See similar remodeling process reported for cartilage construct implanted in Gottingen minipigs (Paetzold et al. 2012) 106

Fig. 2.17 The image shows the base of the radial zone, at the interface with the calcified zone in the rabbit (top image: white arrows highlight three parallel tubes). Bottom image: bases of tubular structures are seen, including orthogonally arranged fibrils apparently binding the 30-nm-diameter collagen fibrils lining the tubules’ walls (arrows). More than a few microns from the interface the collagen structure was entirely disrupted (Gwynn et al. 2002) 107

Fig. 2.18 In the rabbit, well-developed collagen tubes are apparent. Image shows close up of collagen tubes with inner circumferential collagen lining (Gwynn et al. 2002) 108

Fig. 2.19 Scanning electron micrograph of normal 76-year-old femoral head cartilage (imaged in backscatter mode), showing details of osteochondral junction (Li et al. 1999). Scale Bar 100 μm. Note the ribbon-like structures defining collagen sheets 109

Fig. 2.20 High-resolution light micrographs of the deep (i.e. radial) zone in normal human articular cartilage. Images **c** and **d** illustrate typical chondrocyte clusters (chondrons) within the upper **c** and lower **d** halves of the deep zone. As must be apparent from their scant distribution, these cell clusters control huge matrix domains. The arrowheads in **c** and **d** mark the boundary between the pericellular/territorial matrix compartment and the vast interterritorial one. Semithin (1 μm thick) section of Epon-embedded tissue stained with Toluidine Blue 0. Scale bar = 20 μm (Hunziker et al. 2002) 110

Fig. 2.21 **a** Channel indenter pressed into the surface of cartilage (Bevill et al. 2010). **b** High magnification differential interference contrast (DIC) optical image of typical channel relief zone

cartilage microstructure for a surface-intact sample (note that cartilage bulges into channel as cartilage is loaded). Beneath the strain-limiting superficial layer, the periodicity and thickness of oblique shear bands within the cartilage bulge vary with depth. Near the STZ interface (region A), the bands are fine and relatively dense, but band thickness and spacing increase in the deep zone (region B) (*Note* This is a severe non-physiological loading) 112

Fig. 2.22 DIC image sequence of mechanical testing. An isolated native type I collagen fibril from bovine sclera is epoxied to calibrated (57 ± 8 nN/ μ m) glass microneedles, submerged in buffer, and mechanically loaded. Top Gauge length (zero-load). Bottom High-load of 1054 ± 149 nN produces $2.6 \pm 0.3\%$ strain 113

Fig. 2.23 Normalized fractional cutting rate versus applied force per monomer for three size scales. Data is normalized against maximum cutting rate, from the zero-load experimental series, and fit to a single exponential curve (Flynn et al. 2013). *Square* (Camp et al. 2011), *circle* (Zareian et al. 2010). Note that collagenase degradation of a single collagen fiber is close to zero from about 8 pN stress, while collagenase activity reduces to about 20% in whole tissue and 10% for procollagen 114

Fig. 2.24 Differential interference contrast (DIC) optical images of the deformed matrix near the edge of the indenter of intact samples tested in 0.15 M saline. The boxed region in **a** highlights the distinct shear boundary referred to in previous studies as the ‘chevron discontinuity’ 9, 10. **b** DIC image at higher magnification of the boxed region shown in **a**. Note the intense creasing in the upper deformed cartilage layer. **c** SEM image of the smaller boxed region in **b**. The dotted line highlights a force line of action aligned with the creases shown in **b** and reveals an in-phase fibrillar aggregation. **d** SEM image of the larger boxed region shown in **b**. Note the intense fibrillar aggregation, and its dissipation near the shear boundary (Bevill et al. 2010) 116

Fig. 2.25 Transmission electron microscope image of articular cartilage surface in a young dog. Chondrosynovial membrane (i.e. lamina splendens) (\rightarrow) with fine aperiodic fibrils. Bundles of collagen fibers (c) matted together; image magnification $\times 14,000$. Scale bar 1 μ m (Horky and Tichy 2004). 116

Fig. 2.26 Representative histological sections of cartilage explants taken from the interphalangeal joints of horses, incubated with the specific caspase-3 substrate PhiPhiLux G1D2 (green), and counterstained with DAPI (blue), after 12 h of culture. **a** and **b** are unimpacted controls, **c** and **d** suffered a single mechanical

impact and show split in cartilage. **a** and **c** are merge images of DAPI and PhiPhiLux signals, **b** and **d** are PhiPhiLux G1D2 signal only. White arrows point to cells where caspase-3 is active. Original magnification 400 times (Huser et al. 2006). See also Ewers et al. (2001) for extent and depth of surface fracturing. 119

Fig. 2.27 Theoretical arrangement of aggrecan and collagen in cartilage. The aggrecan core protein contains three globular domains including a G3 C-terminal domain, a G2 domain (green), and an N-terminal G1 domain (black). Aggrecan is anchored in the cartilage matrix by binding to link protein (blue diamond) and hyaluronan to form large multimolecular aggregates. Type II collagen fibrils can bind aggrecan in the keratan sulfate-rich region. The figure shows a theoretical arrangement of type II collagen (red) and aggrecan aggregates in which the charged chondroitin sulfate chains of aggrecan protect collagen fibrils from cleavage by collagenases. Another theoretical possibility is that collagen II fibrils bound at the keratan sulfate-rich region obstruct access of aggrecanases to the cleavage site located in the aggrecan interglobular domain between G1 and G2 (Fosang and Beier 2011). Aggrecan keratin sulfate-rich region has moderate affinity for isolated collagen type II (Hedlund et al. 1999) 122

Fig. 2.28 The micrograph clearly demonstrates the interfibrillar bridges (arrows) [note this image is of type I collagen, rather than type II collagen] formed by the decorin side chains. A few chains lie longitudinally along the fibril axis (Raspanti et al. 2008) 123

Fig. 2.29 Collagen fibril and fiber damage [for a ligament] above the damage threshold. Hence, shortly after [5.8% stretch] injury some fibers are intact and appear normal, some fibers are completely ruptured and a ‘gap’ exists between ruptured fibers, and additionally some fibers are intact but contain ruptured collagen fibrils that contain a ‘gap’ between ruptured fibril ends. As such, if the tissue gap remains and is present when new tissue ‘fills in’ without substantial contracture, the repaired fiber or fibril would be longer than its pre-injury length and as such it will be more lax. Magnification 20,000× (Provenzano et al. 2005) 126

Fig. 2.30 Immunochemical localization of type II collagen in an intact articular cartilage region from the knee joint of a 59 year old female with familial OA. mAb 4G9 specifically sees the N-propeptide of collagen type III, which is concentrated in the surface zone and around chondrocytes at depth (Eyre et al. 2006) 129